How to cite: *Angew. Chem. Int. Ed.* **2023**, e202311896
doi.org/10.1002/anie.202311896

Biocatalysis

Manganese Transfer Hydrogenases Based on the Biotin-Streptavidin Technology

Weijin Wang, Ryo Tachibana, Zhi Zou, Dongping Chen, Xiang Zhang, Kelvin Lau, Florence Pojer, Thomas R. Ward, and Xile Hu**

Abstract: Artificial (transfer) hydrogenases have been developed for organic synthesis, but they rely on precious metals. Native hydrogenases use Earth-abundant metals, but these cannot be applied for organic synthesis due, in part, to their substrate specificity. Herein, we report the design and development of manganese transfer hydrogenases based on the biotin-streptavidin technology. By incorporating bio-mimetic Mn(I) complexes into the binding cavity of streptavidin, and through chemo-genetic optimization, we have obtained artificial enzymes that hydrogenate ketones with nearly quantitative yield and up to 98% enantiomeric excess (ee). These enzymes exhibit broad substrate scope and high functional-group tolerance. According to QM/MM calculations and X-ray crystallography, the S112Y mutation, combined with the appropriate chemical structure of the Mn cofactor plays a critical role in the reactivity and enantioselectivity of the artificial metalloenzyme (ArMs). Our work highlights the potential of ArMs incorporating base-meal cofactors for enantioselective organic synthesis.

[*] W. Wang, X. Hu
Laboratory of Inorganic Synthesis and Catalysis, Institute of Chemical Sciences and Engineering, École Polytechnique Fédérale de Lausanne
ISIC-LSCI, BCH 3305, 1015 Lausanne (Switzerland)
E-mail: xile.hu@epfl.ch

R. Tachibana, Z. Zou, D. Chen, X. Zhang, T. R. Ward
Department of Chemistry, University of Basel
Mattenstrasse 22, 4002 Basel (Switzerland)
E-mail: thomas.ward@unibas.ch

K. Lau, F. Pojer
Protein Production and Structure Core Facility (PTPSP), School of Life Sciences, École Polytechnique Fédérale de Lausanne
Lausanne (Switzerland)

T. R. Ward, X. Hu
National Center of Competence in Research (NCCR) Catalysis, EPFL
1015 Lausanne (Switzerland)

Artificial metalloenzymes (ArMs) have emerged as an attractive means to endow organometallic catalysts with an evolvable genotype. ArMs result from the incorporation of a catalytically-competent metallocofactor into a genetically-encoded protein. Several protein scaffolds have proven versatile for assembling and optimizing such hybrid catalysts for transfer hydrogenation reactions.[1] However, these artificial transfer hydrogenases (ATHases) contain a precious metal-based cofactor. In contrast, native metalloenzymes rely primarily on non-noble metal cofactors for catalysis. In terms of hydrogenation, nature uses [Fe]-hydrogenase, which is the only known native enzyme that hydrogenates an organic substrate, namely, methenyl tetrahydromethanopterin (methenyl-H_4MPT^+) (Figure 1A).[2] This reaction is a part of the pathways of microbial methanogenesis.[3] The active site of [Fe]-hydrogenase (Figure 1B) contains an Fe(II) center coordinated to a pyridone derivative, two cis-CO ligands, a cysteine residue, and a water molecule.[4] By incorporation of Fe(II) and Mn(I) complexes mimicking this active site into the apo-protein of [Fe]-hydrogenase, semi-synthetic [Fe]- and [Mn]-hydrogenases have been prepared and shown to exhibit the activity of [Fe]-hydrogenases.[5] However, these hydrogenases, as well as the native [Fe]-hydrogenase, have an exclusive substrate specificity and cannot be used to hydrogenate substrates beyond methenyl-H_4MPT^+.

Manganese, being the third most earth-abundant transition metal, presents a promising and sustainable option for the development of ArMs based on earth-abundant metals. While previous research has explored Mn ArMs in the context of artificial oxidases[6] such as epoxygenases,[7] benzylic oxidases,[8] sulfoxidases,[9] and peroxidases.[10] there remains a notable gap in the availability of Mn ArMs for (transfer) hydrogenation reactions. Here we describe the development of the first base-metal ATHase by incorporating Mn(I) complexes resembling the active site of [Fe]-hydrogenase into the binding pocket of streptavidin (Figure 1C). Through systematic chemo-genetic optimization, we have obtained Mn transfer hydrogenases that exhibit high enantioselectivity, turnover numbers, and broad substrate scope.

We selected Mn as the metal due to its abundance, biocompatibility, and environmentally friendly nature. Compared to their Fe(II) counterparts, Mn(I) complexes are often more stable and easier to handle for incorporation into enzymes.[5b] As for the protein scaffold, we selected streptavidin (Sav), a homotetrameric protein known for its

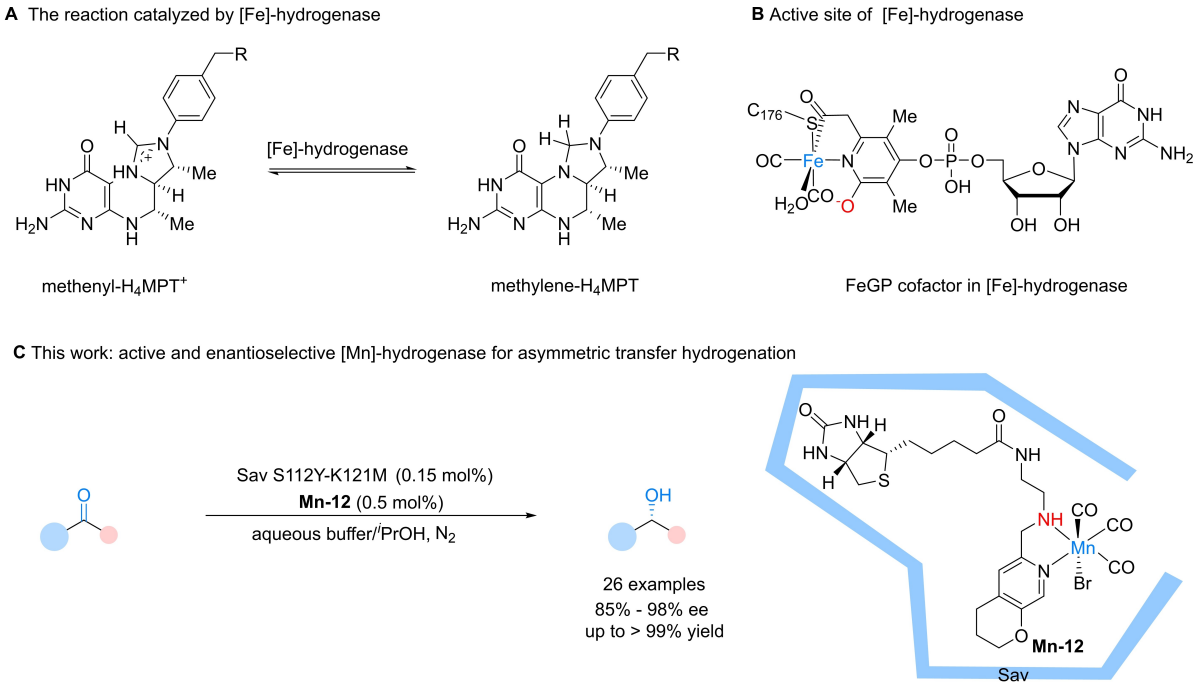

Figure 1. [Fe]-hydrogenase and artificial [Mn] transfer hydrogenase reported in this work. **A**, The reaction of [Fe]-hydrogenase. The [Fe]-hydrogenase catalyzes the reversible hydrogenation of methenyl-H_4MPT^+ in microbial methanogenesis. **B**, The FeGP cofactor in the active site of [Fe]-hydrogenase. The active site contains one Fe(II) center coordinated with a pyridone derivative, two cis-CO ligands, a cysteine residue, and a water molecule. **C**, This work: manganese transfer hydrogenases based on the biotin-streptavidin technology.

high affinity for biotin. In addition, Sav has demonstrated remarkable stability to chaotropic agents, changes in pH, temperature, cosolvent, etc.[11] We initially synthesized two Mn(I) complexes (Figure 2A): one with a bidentate pyridine-2-amine ligand (**Mn-1**) and the other with a tridentate PNN ligand (**Mn-2**), both flanked with a biotin anchor. In **Mn-1**, the anchor was designed to bind to the ligand moiety through an amide bond and an ethylene spacer, while in **Mn-2**, the biotin was reduced to the corresponding alcohol and connected to the tridentate PNN ligand via an ether linkage.

We selected acetophenone **S1** as the substrate and isopropanol as the hydride source. The initial screening was carried out in 0.6 M sodium phosphate buffer at pH 11 at 55 °C for 16 hours. Using wild-type Sav, we observed only minimal activity with **Mn-1** and no activity with **Mn-2** (Figure 2A). Considering previous genetic optimization of ArMs based on the biotin-Sav technology,[1d,11a] we targeted the S112 and K121 residues for saturation mutagenesis, and screened a library of single mutants at both positions. We identified two mutations that greatly enhanced the catalytic performance, both in terms of yield and enantioselectivity. **Mn-1·Sav S112Y** gave a 43 % yield and 81 % ee for the (*R*)-**1** product, while **Mn-1·Sav K121M** gave a 46 % yield and 80 % ee for the same product (Figure 2B).

Over the years, the chemo-genetic optimization has proven its versatility to enhance the catalytic activity of ArMs.[11a,12] Following the screening of single mutants, we set out to fine-tune both the ligand structure and the second coordination sphere around the cofactor by combining beneficial mutations at both positions S112 and K121. Before this, we optimized the temperature, the buffer type and its concentration, reaction time, and cosolvent ratio (Table S1–S5). Next, we synthesized a library of **Mn-1** analogs to explore the structure–activity relationship of the Mn cofactors (Figure 3A). A range of electron-withdrawing and electron-donating groups were introduced at the 5-position of the pyridine ring (**Mn-1**, **3**–**6**). Electron-donating groups, such as –Me (**Mn-5**) and –OMe (**Mn-6**), improved the yield while maintaining a good ee (up to 75 % yield and 85 % ee for **Mn-6**). Substitutions were also evaluated at other positions of the pyridine ring. Shifting the Me substituent from the 5- to 4-position slightly reduced the yield (from **Mn-5** to **Mn-7**). Substitution groups at both the 3- and 5-, or the 6-position significantly reduced the activity (**Mn-8** and **Mn-9**), while the 4- and 5- positions showed competitive results (**Mn-5** to **Mn-7**). Methylation of the amide group has a negligible effect on the reaction outcome (compare **Mn-1** with **Mn-10**), suggesting that the amide group is not involved in catalysis. Based on the above data, we further explored substitutions at the 4- and 5-positions. To this end, two additional Mn complexes were synthesized (**Mn-11** and **Mn-12**). Replacing the pyridine ligand with an isoquinoline ligand improved the ee to 90 %, but at the cost of a reduced yield (49 % for **Mn-11**). We thought that this may be due to the electron-withdrawing nature of the phenyl group. Introducing a tetrahydropyran group -which is electron-donating at the 4- and 5- positions-resulted in enhanced reactivity (**Mn-12**), giving rise to a 95 % yield and 85 % ee, at 0.5 mol% catalyst loading. Next, we combined

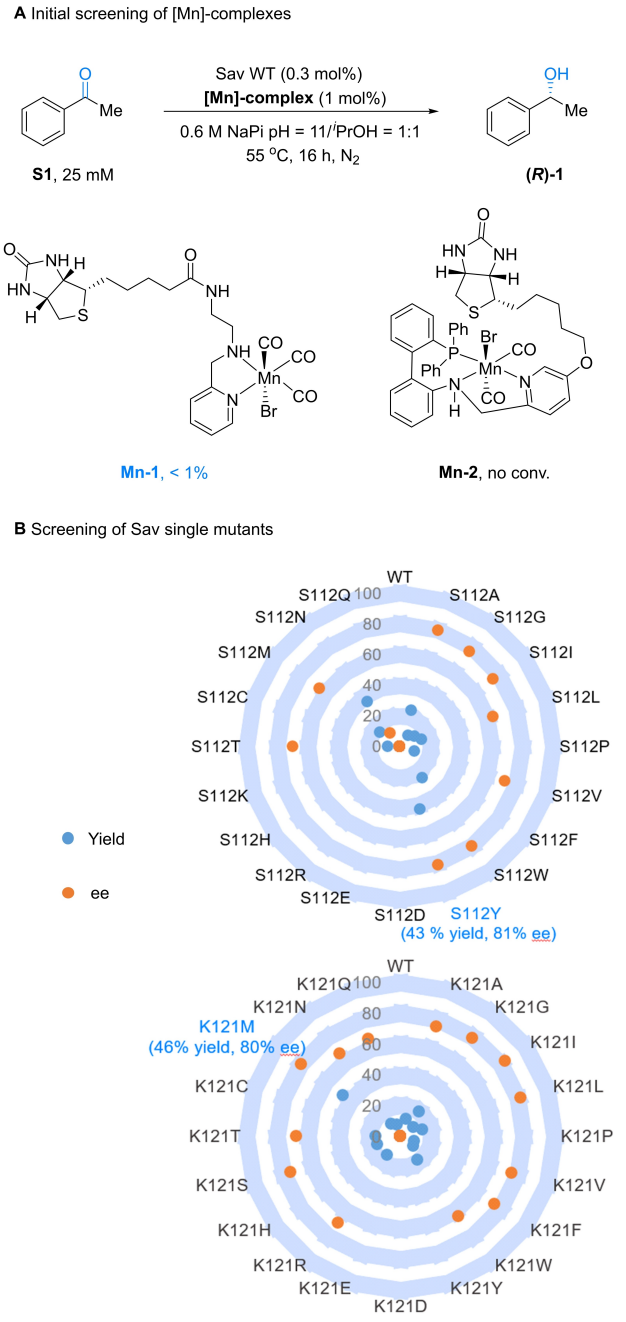

Figure 2. Initial optimization for the transfer hydrogenation of acetophenone **S1**. **A**, Initial screening of [Mn] complexes. Reaction conditions: acetophenone **S1** (25 mM), streptavidin wild-type (75 μM), [Mn]-complex (250 μM), 0.6 M NaPi buffer (pH = 11 200 μL), isopropanol (200 μL), 55 °C, 16 h. **B**, Screening of single mutants. Reaction conditions: acetophenone **S1** (25 mM), streptavidin mutant (75 μM), **Mn-1** (250 μM), 0.6 M NaPi buffer (pH = 11, 200 μL), isopropanol (200 μL), 55 °C, 16 h.

Mn-12 with various Sav double mutants S112Y-K121X or S112X-K121M. Gratifyingly, **Mn-12·Sav S112Y-K121M** provided a 99 % yield and 93 % ee in favor of (*R*)-**1**.

Having identified the cofactor and the host protein, we next explored the substrate scope of aryl ketone substrates (Figure 4) in the presence of **Mn-12·Sav S112Y-K121M**. Initially, we investigated different substitution patterns on the phenyl ring. We were pleased to observe that all *ortho*-, *meta*-, and *para*-substitutions led to high yields and good ee for the corresponding products (**1**–**5**). Under air, we observed a decrease in both the yield and enantioselectivity. Various functional groups, including amine (**6**), hydroxyl (**7**), iodine (**8**), as well as small cycloalkyl groups (**11**,**12**) were tolerated. Notably, the reduction of the cyclopropyl substrate **S11** afforded **11** in 92 % yield. No ring-opened product was detected, suggesting that the reaction proceeds via a hydride transfer rather than a radical mechanism. We also tested alkyl substituents and found that ketones with ethyl (**S9**), isopropyl (**S10**), and cycloalkyl groups (**S11**–**S13**) were reduced in excellent yield and ee. Good results were also obtained for a bicyclic 1-tetralone (**S14**) and an alkenyl ketone (**S15**).

We then tested heteroaryl ketones as substrates. Various heteroarenes, including thiophene (**16**), pyridine (**17**), pyrimidine (**18**), benzofuran (**19**), benzothiophene (**20**), unprotected indole (**21**), benzothiazole (**22**), limidazo[1,2-a]pyridine (**23**), quinoline (**24**) and isoquinoline (**25**) were all hydrogenated even with higher ees compared to aryl ketones. Notably, the isoquinoline was hydrogenated in 98 % ee (**25**). The reaction of an ezetimibe intermediate (**26**) was also efficient. The enantioselectivity of the hydrogenation of a dialkyl ketone, 1-cyclohexyl-2-phenylethan-1-one (**27**) or 1-phenylbutan-2-one (**28**), however, was modest (up to 50 % ee).

Compared with natural enzymes such as alcohol dehydrogenase (ADHs), ADHs exhibit high reactivity and enantioselectivity, efficiently catalyzing both dehydrogenation of alcohols and hydrogenation of ketones.[13] However, their substrate scope is limited. On the other hand, our artificial [Mn]-hydrogenase displays a broader substrate scope, efficiently catalyzing the transfer hydrogenation of various ketones. While the reactivity of this artificial metalloenzyme is generally lower than natural alcohol dehydrogenases, as revealed by the k_{cat}/K_M value of 0.246 (Figure S4). In the meanwhile, compared with synthetic Mn complexes for asymmetric transfer hydrogenation of ketones,[14] our system featured with a competitive substrate scope, higher TON number, lower catalyst loading, aqueous phase reaction and comparable enantioselectivity.

To scrutinize the role of the coordinated NH group in the Mn cofactors, we methylated the N–H in **Mn-1** to afford **Mn-13**. Using **Mn-13·Sav S112Y-K121M** as the catalyst, we obtained no reactivity for the hydrogenation of **S1** (Figure 5A). This result highlights the critical role of the N–H group. We hypothesize that coordinated amine delivers its proton to the substrate, similar to the systems with other synthetic Mn complexes.[15] The system exhibited significant protein accelerated catalysis,[16] as evidence by the following two points: (1) **Mn-12** itself exhibited negligible activity in organic solvents such as isopropanol (Table S7); (2) In the absence of Sav, the free cofactor **Mn-1** and **Mn-12** led to <1% of product **1** (Table S8). Thus, the protein scaffold provides a propitious second coordination sphere environment that significantly affects both the activity and the selectivity of the **Mn-12** cofactor (Figure 5A). The reactions

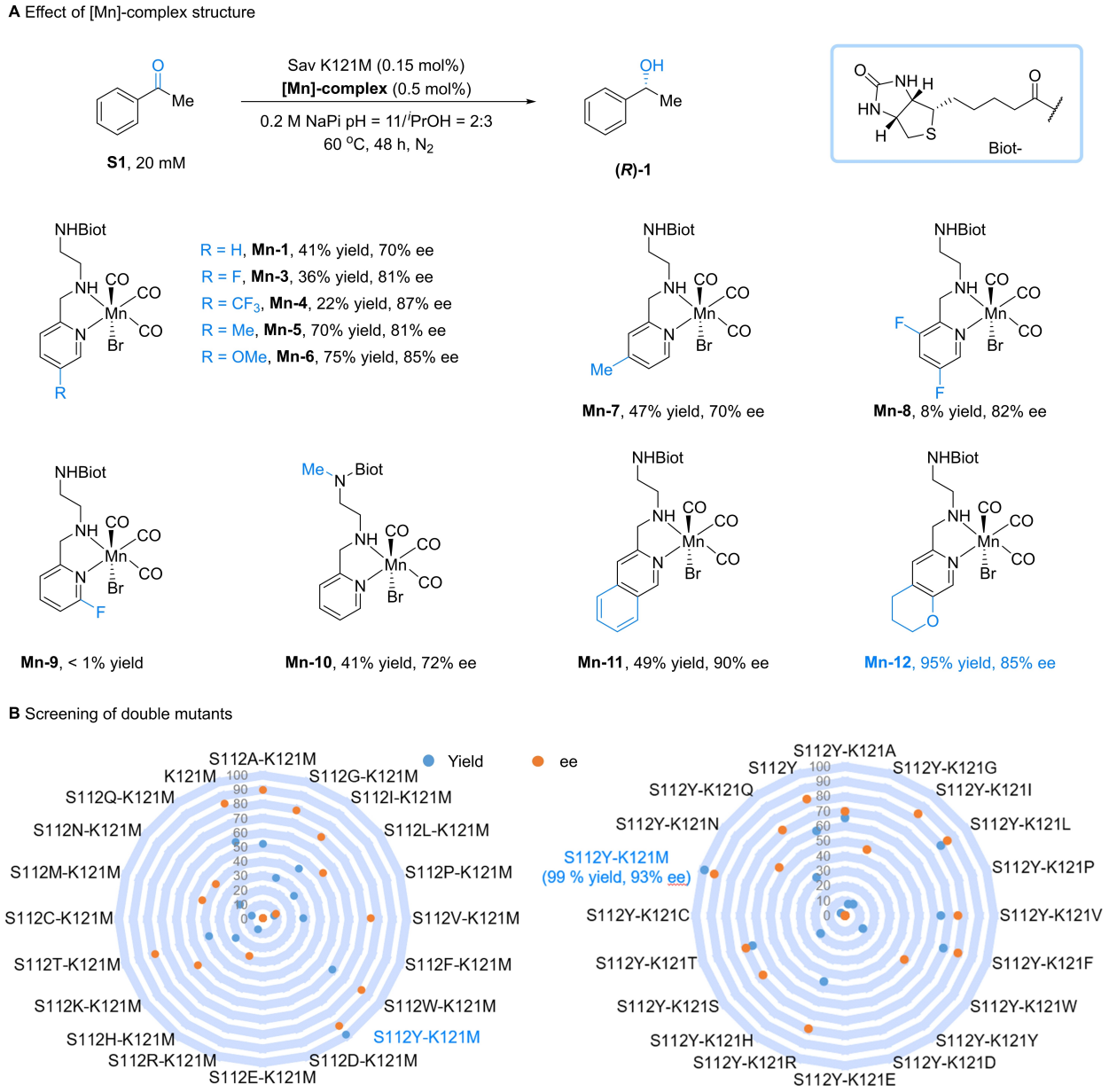

Figure 3. Chemo-genetic optimization of the transfer hydrogenase activity for acetophenone **S1. A**, Effect of cofactor's structure. Reaction conditions: acetophenone **S1** (20 mM), streptavidin K121 M (30 μM), [Mn]-complex (100 μM), 0.2 M NaPi buffer (pH = 11, 200 μL), isopropanol (300 μL), 60 °C, 48 h. **B**, Screening of double mutants in the presence of Mn-12. Reaction conditions: acetophenone **S1** (20 mM), streptavidin double mutant (30 μM), **Mn-12** (100 μM), 0.2 M NaPi buffer (pH = 11, 200 μL), isopropanol (300 μL), 60 °C, 24 h.

are pH sensitive, as they only proceed in the pH range of 10–11.5 (Table S9). Given that the pKa of O–H in tyrosine is ca. 10, we hypothesize that the deprotonated tyrosine S112Y is involved in the catalytic cycle. Besides, only 8 % yield and 50 % ee was obtained with S112F mutation, emphasizing the crucial role of the –OH group in the S112Y mutation (Table S10).

The structures of two complexes, **Mn-5·SavS112Y-K121M** (PDB: 8P5Z) and **Mn-12·SavS112Y-K121M** (PDB: 8P5Y) were solved by X-ray crystallography to atomic resolution (Table S12). For **Mn-12**, the structure was solved to 1.6–1.9 Å by molecular replacement using streptavidin as the template (PDB ID 6J6J); refined to R_{work}/R_{free} 0.19/0.26 which resulted in high quality electron density. The model contains no geometric outliers and a Molprobity score of 1.65. The structure crystallized with one full tetrameric streptavidin-ligand complex in each unit cell. This allowed us to observe four non-equivalent sites of binding in the respective co-crystal structures (Figure S7). Analysis was done on the best-resolved ligand site (Chain B for **Mn-12**). The biotinylated ligands, manganese, and bromide could easily be modeled, as demonstrated by the omit map at the ligand sites (Figure S8 and S9). The S112Y forms a strong π–π interaction between the pyridine moiety on the biotiny-

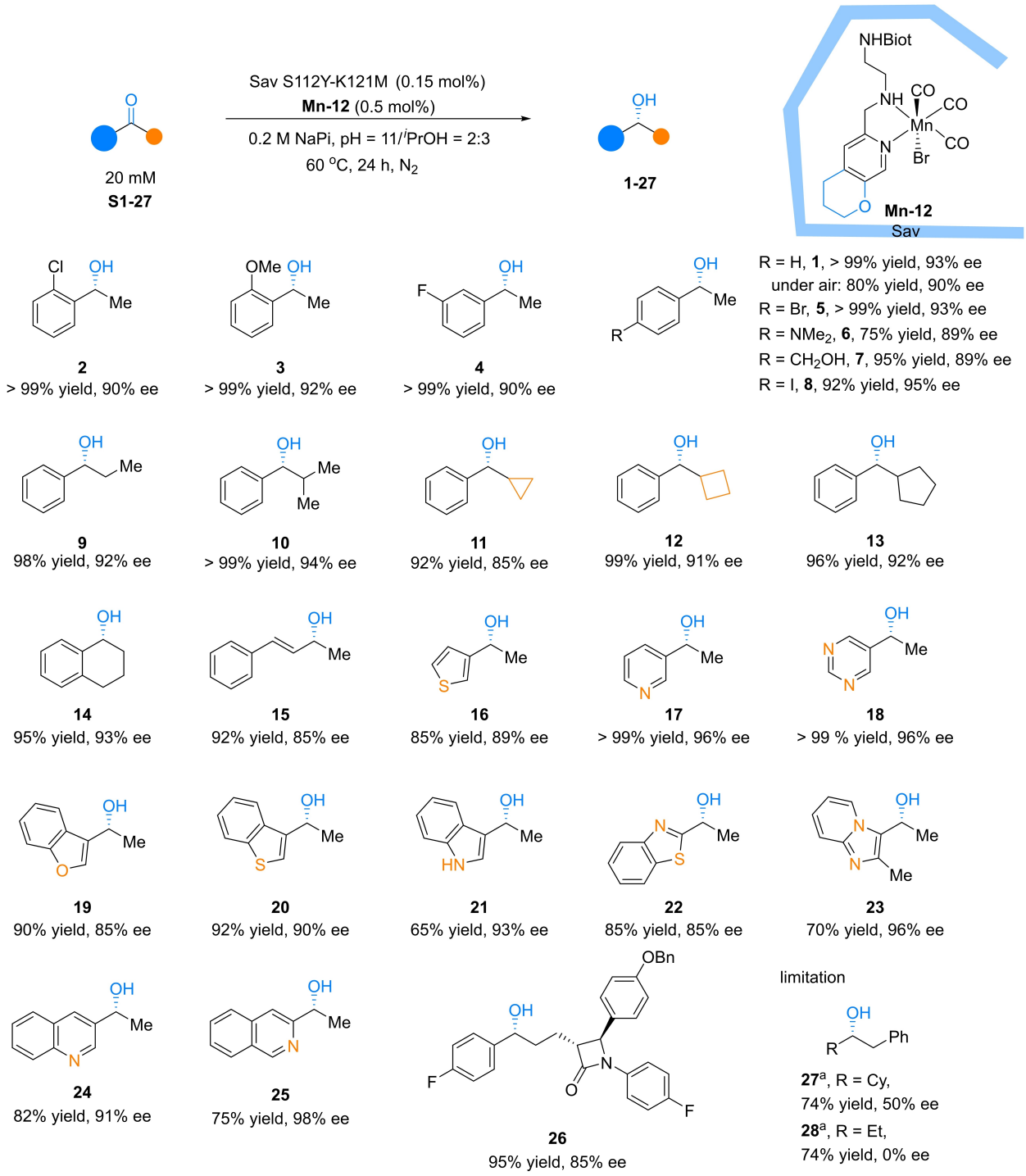

Figure 4. The substrate scope of enantioselective transfer-hydrogenation of ketones by **Mn12·Sav S112Y-K121M**. Reaction conditions: **S2**–**S26** (20 mM), streptavidin S112Y-K121 M (30 μM), **Mn-12** (100 μM), 0.2 M NaPi buffer (pH = 11, 200 μL), isopropanol (300 μL), 60 °C, 24 h. [a]Reaction conditions: **S27** or **S28** (10 mM), streptavidin mutants (30 μM), **Mn-12** (100 μM), 0.2 M NaPi buffer (pH = 11, 200 μL), isopropanol (300 μL), 60 °C, 48 h.

lated ligands (Figure 5B, distance 3.4 Å for **Mn-12**). Two M121 residues coming from adjacent monomers are sandwiched between two ligands. Unfortunately, we were unable to accurately place the carbon monoxides, although there are some density features at some of the ligands to support their presence (Figure S8). It is possible that under long incubation time in the aqueous phase for the crystallization, the carbon monoxide ligands may be partially replaced by water molecules.

To complement the X-ray crystallography, we conducted quantum mechanics/molecular mechanics (QM/MM) calculations to model the structure of **Mn-12·Sav S112Y-K121M**

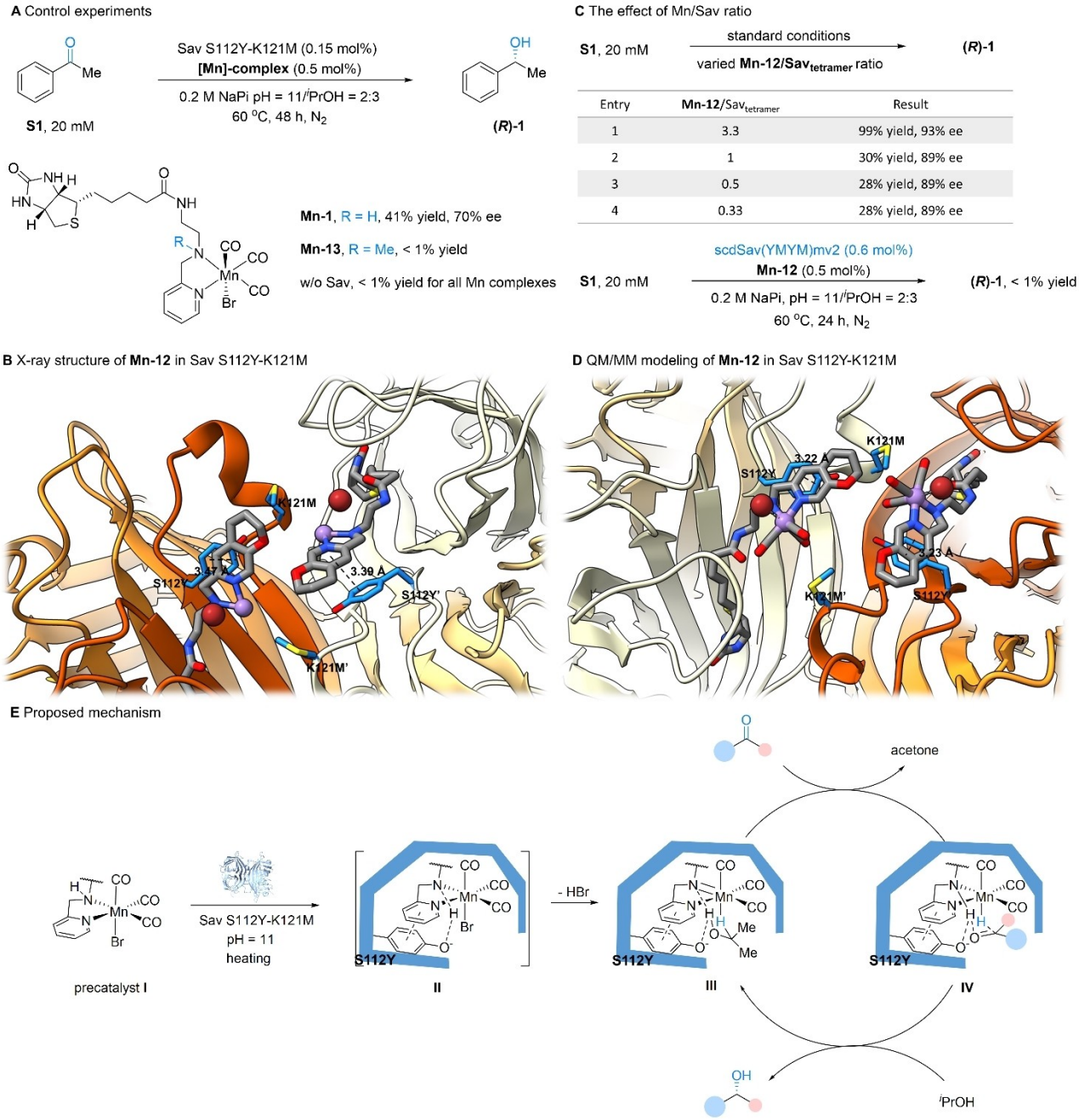

Figure 5. Mechanistic and structural studies. **A**, Control experiments. The result suggests that the N–H is crucial for the reactivity, indicating a cooperative mechanism. Besides, a strong protein-accelarated catalysis was observed, indicating possible interaction between the amino acid residue and the Mn cofoactors. **B**, Close-up view of the crystal structure of **Mn-12·Sav S112Y-K121M** (PDB: 8P5Y). Sav is displayed as a cartoon representation of the two 8-stranded β-barrels forming the biotin-binding vestibule. Close-lying residues and the Mn cofactors are displayed as color-coded sticks, Mn as a purple sphere and Br as a red sphere. Each monomer is coloured differently. Ligands are coloured in grey. Mutations of interest are colorued in Blue. **C**, The effect of Mn/Sav ratio. A smaller Mn:$Sav_{tetramer}$ ratio resulted in decreased catalytic activity, suggesting that the close interaction between two Mn complexes may contribute to improved reactivity. **D**, QM/MM modeling of **Mn-12·Sav S112Y-K121M**. **E**, Proposed mechanism. Under the reaction conditions (pH = 11), the tyrosine residue S112Y is mostly deprotonated. This residue can serve as a Bronsted base to facilitate the proton transfer in the catalytic cycle, highlighting the critical role of the -OH.

(Figure 5D). The calculation result supports the formation of a π–π stacking interaction between the pyridine ring on the ligand and the phenyl ring of the tyrosine residue (Figure 5D), which favors the localization of Mn complex. An unexpected, yet interesting observation is the close interaction between two neighboring Mn complexes, with the shortest contact between the closest oxygen atoms of the pyridone ligands (Figure 5 B,D). We hypothesize that this close interaction may contribute to improved reactivity and enantioselectivity observed in **Mn-12·Sav S112Y-K121M**. To

support this hypothesis, we initially varied the ratio of free binding sites to the Mn cofactor during the reaction (Figure 5C). Remarkably, when compared to the standard conditions, which yielded an impressive 99 % yield and 93 % ee (Figure 5C, entry 1), we observed that a smaller Mn: $Sav_{tetramer}$ ratio resulted in decreased catalytic activity. And further increasing the protein loading beyond a ratio of 1, where only one Mn cofactor binds to each Sav tetramer, had no significant impact on the catalysis outcome (Figure 5C, entries 2–4). Furthermore, we expressed a single chain dimer streptavidin bearing the S112Y-K121 M mutations, with one biotin binding vestibule inactivated by additional N23A/S27D/D128A mutations[17] (scdSav(YMYM)mv2). When this protein was used as the host, no conversion of acetophenone was observed (Figure 5C). Based on these results, we propose that the precise localization of the **Mn-12** and its interaction with S112Y play a crucial role in the outcome of catalysis.

Previous studies report a cooperative mechanism for the Mn ions and a basic moiety in its coordination sphere for hydrogenation reactions catalyzed by Mn(I) complexes[15,18]. Our data suggest a similar mechanism (Figure 5E). Under the reaction conditions (pH = 11), the tyrosine residue S112Y is mostly deprotonated. This residue can serve as a Bronsted base to facilitate the proton transfer in the catalytic cycle: i) It may aid in eliminating HBr from the precatalyst to form the active form of catalyst (**III**). ii) the tyrosinate might aid the transfer of the proton from isopropanol to the N^- coordinated to Mn, or the transfer of the proton from NH in **IV** to the ketone.

In conclusion, we have designed and evolved an efficient Mn ATHase based on the biotin-streptavidin technology. These base-metal containing ArMs exhibit high activity and enantioselectivity for the reduction of a wide range of aryl ketones. Both the structural optimization of Mn cofactors and the genetic optimization of Sav proved critical in rapidly identifying a proficient ATHase. X-ray crystallography and QM-MM computations provide insight into the critical role of the Sav S112Y mutation. To the best of our knowledge, the Mn ArM presented herein is the first example of base-metal containing transfer-hydrogenase. Their high activity, broad substrate scope, and high functional group tolerance underscore the potential of base-metal ArMs in organic synthesis. Efforts are currently underway to improve the results for dialkyl ketone substrates.

Supporting Information

Experimental procedures, and compound characterization data that support the findings of this study are available in the online version of this paper in the accompanying Supporting Information. The data supporting this study are available online in Zenodo: doi: 10.5281/zenodo.8312813.

Acknowledgements

The work in EPFL-LSCI is supported by the Swiss National Science Foundation (no. 200020_212062). This publication was created as part of NCCR Catalysis (grant number 180544), a National Centre of Competence in Research funded by the Swiss National Science Foundation. RT thanks the Naito Foundation for financial support. XZ thanks the SIOC for a postdoctoral scholarship. We thank in particular Amédé Larabi (PTPSP) for screening and optimizing the crystallization conditions and Dr. Huijie Pan (EPFL) for preliminary studies. Open Access funding provided by École Polytechnique Fédérale de Lausanne.

Conflict of Interest

The authors declare no conflict of interest.

Data Availability Statement

The data that support the findings of this study are openly available in Zenodo at https://doi.org/10.5281/zenodo.8312813. The crystal structures of two proteins, **Mn-5·SavS112Y-K121M** (PDB: 8P5Z) and **Mn-12·SavS112Y-K121M** (PDB: 8P5Y) are openly available in RCSB Protein Data Bank (RCSB PDB).

Keywords: Biocatalysis · Hydrogenases · Hydrogenation · Manganese · Metalloenzyme

[1] a) M. E. Wilson, G. M. Whitesides, *J. Am. Chem. Soc.* **1978**, *100*, 306–307; b) A. Stein, D. Chen, N. V. Igareta, Y. Cotelle, J. G. Rebelein, T. R. Ward, *ACS Cent. Sci.* **2021**, *7*, 1874–1884; c) C. Letondor, N. Humbert, T. R. Ward, *Proc. Natl. Acad. Sci. USA* **2005**, *102*, 4683–4687; d) J. Zhao, J. G. Rebelein, H. Mallin, C. Trindler, M. M. Pellizzoni, T. R. Ward, *J. Am. Chem. Soc.* **2018**, *140*, 13171–13175; e) M. Pellizzoni, G. Facchetti, R. Gandolfi, M. Fusè, A. Contini, I. Rimoldi, *ChemCatChem* **2016**, *8*, 1665–1670; f) G. Facchetti, I. Rimoldi, *New J. Chem.* **2018**, *42*, 18773–18776; g) D. S. Mérel, S. Gaillard, T. R. Ward, J.-L. Renaud, *Catal. Lett.* **2016**, *146*, 564–569; h) K. Kariyawasam, W. Ghattas, Y. L. De Los Santos, N. Doucet, S. Gaillard, J.-L. Renaud, F. Avenier, J.-P. Mahy, R. Ricoux, *Biotechnol. Appl. Biochem.* **2020**, *67*, 563–573; i) A. Chevalley, M. Salmain, *Chem. Commun.* **2012**, *48*, 11984–11986; j) M. V. Cherrier, S. Engilberge, P. Amara, A. Chevalley, M. Salmain, J. C. Fontecilla-Camps, *Eur. J. Inorg. Chem.* **2013**, 3596–3600; k) J. de Jesús Cázares-Marinero, C. Przybylski, M. Salmain, *Eur. J. Inorg. Chem.* **2018**, 1383–1393; l) A. Chevalley, M. V. Cherrier, J. C. Fontecilla-Camps, M. Ghasemi, M. Salmain, *Dalton Trans.* **2014**, *43*, 5482–5489; m) D. J. Raines, J. E. Clarke, E. V. Blagova, E. J. Dodson, K. S. Wilson, A.-K. Duhme-Klair, *Nat. Catal.* **2018**, *1*, 680–688.
[2] S. Shima, U. Ermler, *Eur. J. Inorg. Chem.* **2011**, 963–972.
[3] L. Bai, T. Fujishiro, G. Huang, J. Koch, A. Takabayashi, M. Yokono, A. Tanaka, T. Xu, X. Hu, U. Ermler, S. Shima, *Faraday Discuss.* **2017**, *198*, 37–58.
[4] G. Huang, T. Wagner, M. D. Wodrich, K. Ataka, E. Bill, U. Ermler, X. Hu, S. Shima, *Nat. Catal.* **2019**, *2*, 537–543.

[5] a) S. Shima, D. Chen, T. Xu, M. D. Wodrich, T. Fujishiro, K. M. Schultz, J. Kahnt, K. Ataka, X. Hu, *Nat. Chem.* **2015**, *7*, 995–1002; b) H.-J. Pan, G. Huang, M. D. Wodrich, F. F. Tirani, K. Ataka, S. Shima, X. Hu, *Nat. Chem.* **2019**, *11*, 669–675; c) H.-J. Pan, G. Huang, M. D. Wodrich, F. F. Tirani, K. Ataka, S. Shima, X. Hu, *Angew. Chem. Int. Ed.* **2021**, *60*, 13350–13357.
[6] F. Schwizer, Y. Okamoto, T. Heinisch, Y. Gu, M. M. Pellizzoni, V. Lebrun, R. Reuter, V. Köhler, J. C. Lewis, T. R. Ward, *Chem. Rev.* **2018**, *118*, 142–231.
[7] a) K. Okrasa, R. J. Kazlauskas, *Chem. Eur. J.* **2006**, *12*, 1587–1596; b) E. Sansiaume, R. Ricoux, D. Gori, J.-P. Mahy, *Tetrahedron: Asymmetry* **2010**, *21*, 1593–1600.
[8] a) C. Zhang, P. Srivastava, K. Ellis-Guardiola, J. C. Lewis, *Tetrahedron* **2014**, *70*, 4245–4249; b) K. Oohora, Y. Kihira, E. Mizohata, T. Inoue, T. Hayashi, *J. Am. Chem. Soc.* **2013**, *135*, 17282–17285; c) K. Oohora, H. Meichin, Y. Kihira, H. Sugimoto, Y. Shiro, T. Hayashi, *J. Am. Chem. Soc.* **2017**, *139*, 18460–18463.
[9] a) A. Mahammed, Z. Gross, *J. Am. Chem. Soc.* **2005**, *127*, 2883–2887; b) J. R. Carey, S. K. Ma, T. D. Pfister, D. K. Garner, H. K. Kim, J. A. Abramite, Z. Wang, Z. Guo, Y. Lu, *J. Am. Chem. Soc.* **2004**, *126*, 10812–10813; c) A. Pordea, D. Mathis, T. R. Ward, *J. Organomet. Chem.* **2009**, *694*, 930–936.
[10] a) U. Markel, D. F. Sauer, M. Wittwer, J. Schiffels, H. Cui, M. D. Davari, K. W. Kröckert, S. Herres-Pawlis, J. Okuda, U. Schwaneberg, *ACS Catal.* **2021**, *11*, 5079–5087; b) K. Kariyawasam, T. Di Meo, F. Hammerer, M. Valerio-Lepiniec, G. Sciortino, J.-D. Maréchal, P. Minard, J.-P. Mahy, A. Urvoas, R. Ricoux, *Chem. Eur. J.* **2020**, *26*, 14929–14937.
[11] a) T. R. Ward, *Acc. Chem. Res.* **2011**, *44*, 47–57; b) T. Heinisch, T. R. Ward, *Acc. Chem. Res.* **2016**, *49*, 1711–1721; c) A. D. Liang, J. Serrano-Plana, R. L. Peterson, T. R. Ward, *Acc. Chem. Res.* **2019**, *52*, 585–595.
[12] a) G. Klein, N. Humbert, J. Gradinaru, A. Ivanova, F. Gilardoni, U. E. Rusbandi, T. R. Ward, *Angew. Chem. Int. Ed.* **2005**, *44*, 7764–7767; b) B. Large, N. G. Baranska, R. L. Booth, K. S. Wilson, A.-K. Duhme-Klair, *Curr. Opin. Green Sustain. Chem.* **2021**, *28*, 100420.
[13] a) A. A. Koesoema, D. M. Standley, T. Senda, T. Matsuda, *Appl. Microbiol. Biotechnol.* **2020**, *104*, 2897–2909; b) Z. Li, H. Yang, J. Liu, Z. Huang, F. Chen, *Chem. Rec.* **2021**, *21*, 1611–1630; c) M. M. Musa, R. S. Phillips, *Catal. Sci. Technol.* **2011**, *1*, 1311–1323; d) W. Kroutil, H. Mang, K. Edegger, K. Faber, *Curr. Opin. Chem. Biol.* **2004**, *8*, 120–126.
[14] a) L. Wang, J. Lin, Q. Sun, C. Xia, W. Sun, *ACS Catal.* **2021**, *11*, 8033–8041; b) A. Zirakzadeh, S. R. M. M. de Aguiar, B. Stöger, M. Widhalm, K. Kirchner, *ChemCatChem* **2017**, *9*, 1744–1748; c) K. Z. Demmans, M. E. Olson, R. H. Morris, *Organometallics* **2018**, *37*, 4608–4618; d) D. Wang, A. Bruneau-Voisine, J.-B. Sortais, *Catal. Commun.* **2018**, *105*, 31–36; e) K. Azouzi, A. Bruneau-Voisine, L. Vendier, J.-B. Sortais, S. Bastin, *Catal. Commun.* **2020**, *142*, 106040; f) G.-Y. Zhang, S.-H. Ruan, Y.-Y. Li, J.-X. Gao, *Chin. Chem. Lett.* **2021**, *32*, 1415–1418.
[15] K. Das, S. Waiba, A. Jana, B. Maji, *Chem. Soc. Rev.* **2022**, *51*, 4386–4464.
[16] J. Collot, N. Humbert, M. Skander, G. Klein, T. R. Ward, *J. Organomet. Chem.* **2004**, *689*, 4868–4871.
[17] S. Wu, Y. Zhou, J. G. Rebelein, M. Kuhn, H. Mallin, J. Zhao, N. V. Igareta, T. R. Ward, *J. Am. Chem. Soc.* **2019**, *141*, 15869–15878.
[18] a) S. Elangovan, C. Topf, S. Fischer, H. Jiao, A. Spannenberg, W. Baumann, R. Ludwig, K. Junge, M. Beller, *J. Am. Chem. Soc.* **2016**, *138*, 8809–8814; b) F. Kallmeier, T. Irrgang, T. Dietel, R. Kempe, *Angew. Chem. Int. Ed.* **2016**, *55*, 11806–11809; c) R. Buhaibeh, O. A. Filippov, A. Bruneau-Voisine, J. Willot, C. Duhayon, D. A. Valyaev, N. Lugan, Y. Canac, J.-B. Sortais, *Angew. Chem. Int. Ed.* **2019**, *58*, 6727–6731; d) M. Glatz, B. Stöger, D. Himmelbauer, L. F. Veiros, K. Kirchner, *ACS Catal.* **2018**, *8*, 4009–4016; e) L. Zhang, Y. Tang, Z. Han, K. Ding, *Angew. Chem. Int. Ed.* **2019**, *58*, 4973–4977; f) R. van Putten, E. A. Uslamin, M. Garbe, C. Liu, A. Gonzalez-de-Castro, M. Lutz, K. Junge, E. J. M. Hensen, M. Beller, L. Lefort, E. A. Pidko, *Angew. Chem. Int. Ed.* **2017**, *56*, 7531–7534.

Manuscript received: August 15, 2023
Accepted manuscript online: September 6, 2023
Version of record online: ■■, ■■

Communications

Biocatalysis

W. Wang, R. Tachibana, Z. Zou, D. Chen, X. Zhang, K. Lau, F. Pojer, T. R. Ward,* X. Hu* _____ **e202311896**

Manganese Transfer Hydrogenases Based on the Biotin-Streptavidin Technology

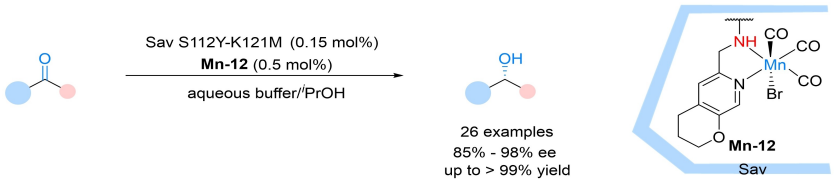

Efficient Mn artificial transfer hydrogenases (ATHases) were developed using the biotin-streptavidin technology, which exhibits high activity and enantioselectivity for the transfer hydrogenation of a wide range of aryl ketones. The S112Y-K121 M double mutation and the appropriate chemical structure of the Mn cofactor play critical roles in the reactivity and enantioselectivity of the enzymes.